Available online at www.sciencedirect.com

ScienceDirect

Procedia Structural Integrity 79 (2026) 1–8

Structural Integrity Procedia

www.elsevier.com/locate/procedia

28th International Conference on Fracture and Structural Integrity - 3rd Mediterranean Conference on Fracture and Structural Integrity

Microstructure and mechanical properties of two quenched and tempered steels for industrial undercarriage track links: A preliminary comparison

Lorenzo Antonioli[a,*], Chiara Soffritti[a], Cindy Morales[a], Denis Benasciutti[b], Elena Capatti[c], Mattia Merlin[a]

[a]*University of Ferrara, Department of Engineering (DE), Via Saragat 1, Ferrara 44122, Italy*
[b]*University of Udine, Polytechnic Department of Engineering and Architecture (DPIA), Via delle Scienze 206, Udine 33100, Italy*
[c]*BERCO S.p.A., Via I Maggio 237, Copparo (FE) 44034, Italy*

Abstract

Thanks to their resistance to static and fatigue loads, quenched and tempered (Q&T) steels are widely used to produce track links for undercarriage systems of industrial machines, which operate under severe mechanical and environmental conditions. This preliminary study investigates the fatigue properties of two Q&T forged steels: the 27MnCrB5-2 steel subjected to a low-temperature tempering treatment to reduce the environmental impact of industrial production, and the carbon-neutral 36CTR4 steel tempered at a higher temperature. Tensile and rotating bending fatigue tests were carried out on specimens directly extracted from heat-treated track links. Static properties enabled a preliminary calibration of the stress amplitude levels for fatigue testing, while microstructural characterization by optical microscopy (OM) and scanning electron microscopy (SEM) was performed to understand the influence of microstructure on the fatigue properties of the investigated steels. Preliminary fatigue data were analyzed using a bi-conditional probability–stress–life (P-S-N) model, enabling a robust statistical evaluation of fatigue resistance. The results confirmed the effectiveness of the selected heat treatments in ensuring reliable mechanical performance.

Keywords: quenched and tempered steels; rotating bending fatigue; heavy-duty applications; microstructure

* Corresponding author. Tel.: +39-345-127-0135.
E-mail address: lorenzo.antonioli@unife.it

10.1016/j.prostr.2025.12.302

1. Introduction

Quenched and tempered (Q&T) steels are widely employed in the manufacturing of components used in sectors such as mining, civil construction, and defense, as reported by Valtonen et al. (2019). The severe working environmental conditions of such applications – e.g. high static, cyclic, impulsive loads, and wear – require metals with a suitable combination of mechanical properties. Lath martensite is the most typical microstructure of low- and medium-carbon steels after quenching (Speich et al. (1972)). Although it is well known that martensite determines a high level of hardness and strength, this phase is rarely exploited in non-tempered condition due to its lack of ductility and toughness, which is caused by the internal stresses associated with the transformation of martensite from the parent austenite phase (Lee et al. (1999)). Hence, after forging, quenched low- and medium-carbon steels are tempered to obtain a microstructure characterized by adequate strength, toughness and fatigue resistance.

The Q&T steels are usually alloyed with elements such as Boron (B) and Molybdenum (Mo). As highlighted by Shigesato et al. (2014), and Li et al. (2015), B is an efficient alloying element since it increases strength and improves hardenability of steels; especially, B retards and/or prevents the nucleation of softer ductile phases such as ferrite, improving hardenability. Concerning Mo, it is usually added to steels to promote the formation of phases such as bainite and martensite (Mohrbacher (2018)), and a synergic effect with B is widely reported in literature (Mohrbacher, 2018; Larrañaga-Otegui et al. (2016)). Indeed, the hardenability effect of Mo is complementary to that of B since Mo segregates to the austenite grain boundaries and retards the formation of ferrite.

The selected heat treatment parameters and the addition of alloying elements govern the final microstructure and, consequently, the mechanical response of Q&T steels. Regarding fatigue resistance, some researchers investigated the fatigue properties of Q&T steels and found that the most important factors affecting the mechanical performance are tempering temperature and duration. London et al. (1989) observed that a Q&T 4140 steel exhibited an improvement of fatigue life by increasing the tempering temperature up to 700 °C, because of a reduced growth rate of small cracks. By contrast, Li et al. (2017) reported the opposite trend for a 0.44 wt. % C steel under rotating bending fatigue conditions.

The present study investigates the fatigue behavior of two medium-carbon steels, usually employed in the manufacturing of undercarriage track links of industrial machines exposed to heavy-duty applications. The aim of this preliminary study is to compare the microstructure and the mechanical properties, i.e., tensile strength, hardness, and fatigue resistance of both steels using specimens directly extracted from forged components, which are heat-treated according to different tempering temperatures. Especially, the investigation focuses on how the selected heat treatment parameters – and consequently, the resulting microstructure – affects the fatigue resistance of the material.

2. Experimental Activities

2.1. Materials

Several track links, made of 27MnCrB5-2 and 36CTR4 medium-carbon steels, were produced from billets forged in a hydraulic press. Specifically, the 36CTR4 steel investigated in this study is a carbon neutral steel, hence produced by balancing CO_2 emissions. The chemical composition of the steels was measured using the LECO CS744 and TC400 (LECO Corporation, St. Joseph, MI, USA) elemental analyzers and is reported in Table 1.

Table 1. Chemical composition (wt. %) of the steels examined.

Steel	Fe	C	Mn	Si	Cr	S	P	Mo	Al	Cu	Ti	Ni	B
27MnCrB5-2	Balance	0.29	1.3	0.3	0.35	0.009	0.02	0.02	0.02	0.24	0.05	0.1	0.002
36CTR4	Balance	0.34	1.12	0.28	0.16	0.026	0.014	0.03	0.027	0.18	0.05	0.12	0.003

After forging, the track links were water quenched and then tempered in an industrial furnace. Tempering temperatures for the 27MnCrB5-2 and 36CTR4 steels were set in the range of 150÷250 °C, and 450÷550 °C, respectively. The geometry of the track links is reported in Figure 1; the black-dotted boxes in the figure depict the zones of the component from which raw cylindrical samples were extracted for conducting the experimental activities

of the present study. The cylindrical samples were machined to obtain at least three tensile specimens and fifteen fatigue specimens for each steel. Proportional tensile specimens with a specific gauge length/diameter ratio were machined in agreement with the ASTM E8/E8M (2021) standard, while the fatigue specimens were prepared according to the ASTM E466 (2021) one.

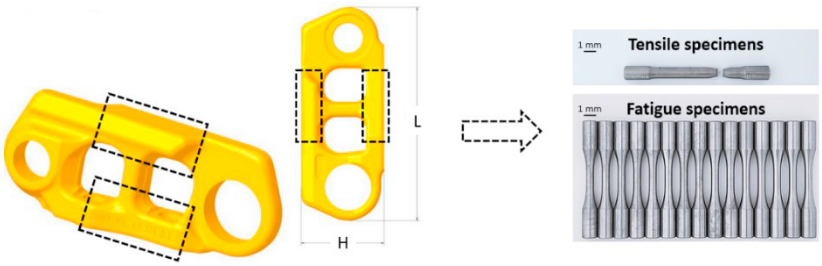

Fig. 1: Example of undercarriage track links used for the purposes of the present investigation. Tensile and fatigue specimens were extracted from the zones enclosed in the black-dotted boxes.

2.2. Tensile and Hardness Testing

The tensile tests were performed according to the ISO 6892-1 (2019) standard by an MTS 810 (MTS Systems Corporation, Minneapolis, MN, USA) electromechanical testing machine with a 100 kN loading cell. The tensile properties, including the yield strength (YS), the ultimate tensile strength (UTS), the elongation at fracture (A%), and the reduction of area at fracture (Z%) were directly determined form the software implemented in the testing machine.

Vickers hardness tests were performed according to the ISO 6507-1 (2023) standard by a Qness 60 CHD MASTER+ (QATM, Golling, Austria) equipment, with a load of 9.807 N and a square-based pyramidal indenter. At least fifteen measurements were performed on both the longitudinal and transversal cross-sections of the tensile specimens.

2.3. Fatigue Testing

Rotating bending fatigue tests (stress ratio $R = -1$) were performed on a RB35 (Italsigma, Forlì, Italy) electromechanical machine. Fatigue tests were conducted at frequency of 50 Hz and at room temperature. A maximum of two fatigue tests were performed under each constant stress amplitude, and test survival (run out) was set to 5 million cycles. Subsequent statistical analysis of experimental results was performed using a bi-conditional probability-stress-life (P-S-N) model taken from the literature (Cova & Tovo (2017)). The model considers both the inclined portion of the stress-life (S-N) line and a randomly distributed fatigue limit, and provides the scatter bands for assigned values of the probability of failure P_f. The S-N curves for the investigated Q&T steels were estimated using a purpose-built R2024b MATLAB code.

2.4. Microstructural and Fractographic Analyses

The fracture surfaces of the fatigue specimens were investigated by a Zeiss EVO MA 15 (Carl Zeiss Microscopy, Jena, Germany) scanning electron microscope (SEM), equipped with a lanthanum hexaboride (LaB_6) emitter, with an accelerating voltage ranging from 15 to 20 kV. The microscope was also coupled to an Oxford X-Max 50 (Oxford Instruments, Abingdon-on-Thames, UK) energy dispersive microprobe for semi-quantitative analyses (EDS). The SEM micrographs were recorded in both secondary electrons (SE) imaging and backscattered electrons (BSE) imaging.

Metallographic samples were cut out perpendicularly to the fracture surfaces of the tensile specimens, embedded in a conductive resin, and prepared according to standard grinding and polishing procedures. The Nital 2 vol. % etchant (2 % solution of nitric acid in ethanol) was used for qualitative metallography performed in bright field observation mode on a Leica DMi8A (Leica Microsystems, Wetzlar, Germany) optical microscope (OM) coupled to the LAS v4.13 software.

3. Results and Discussions

3.1. Microstructural Analyses

Figure 2a shows the microstructure of the 27MnCrB5-2 steel and as expected, evidence of a needle-like phase consistent with a second stage tempered martensite can be observed. Similar findings were highlighted also by Bastidas et al. (2021) for quenched and tempered steel components made of 27MnCrB5-2 steel. Figure 2b displays the microstructure of the 36CTR4 steel, where the presence of a sorbitic microstructure can be noted. Comparable results were reported by Croccolo et al. (2013) for a similar steel used for manufacturing track chains of high-power excavators and tempered at high temperature.

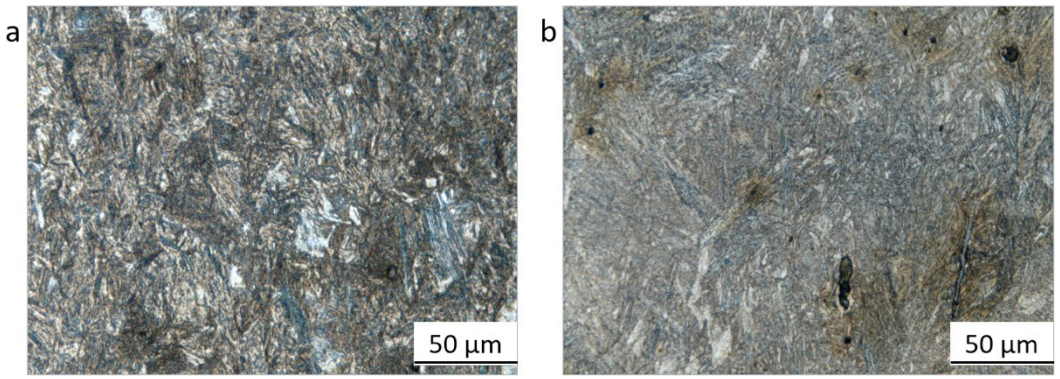

Fig. 2: OM micrographs (500× magnification) showing the microstructure of (a) 27MnCrB5-2 and (b) 36CTR4 steels.

3.2. Mechanical Properties

Figure 3 collects the mean values of the experimental results from tensile and hardness tests. As concerns the tensile strength of the 36CTR4 steel, a decrease of about 30 % and 22 % in UTS and YS was highlighted with respect to the 27MnCrB5-2 one (Figure 3a). Thus, tempering carried out on the as-quenched 27MnCrB5-2 steel reduced internal stresses of martensite without significantly reducing its strength, as also emphasized by Dudko et al. (2022) for a 0.4 wt.% C Q&T steel. On the other hand, the 36CTR4 steel exhibits an increase of about 14 % and 5 % in A% and Z%, respectively, because of the tempering performed at higher temperature (Figure 3b). Moreover, the hardness values (Figure 3c) measured on both longitudinal and transversal cross-sections of tensile specimens are almost comparable, though hardness is greater for the 27MnCrB5-2 steel in agreement with the UTS (see Figure 3a).

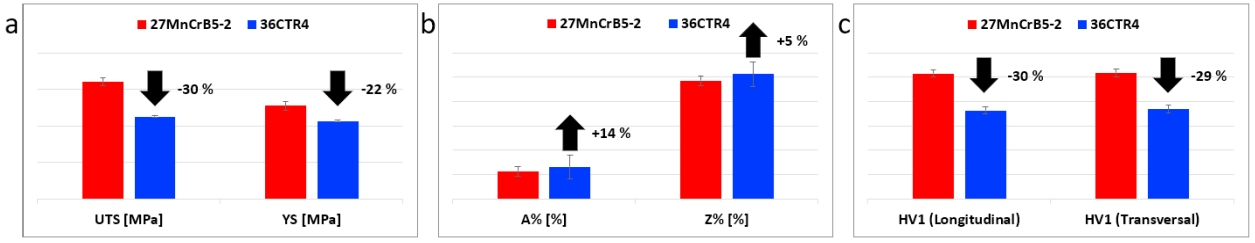

Fig. 3: Mean values of (a) UTS and YS, (b) A% and Z%, (c) HV1 hardness of the 27MnCrB5-2 and 36CTR4 steels. The values of the estimated standard deviation are reported as error bars. Values are intentionally masked to protect intellectual property.

Figure 4 compares the mean fatigue curves ($P_f = 50$ %) of the investigated Q&T steels, along with the scatter bands for P_f = 1% and 99% failure probability. In agreement with the experimental findings of Li et al. (2017), the 27MnCrB5-2 steel exhibits an improved fatigue resistance with respect to the 36CTR4 one, both in low- and high-cycle regions. Compared to the 36CTR4 steel, the 27MnCrB5-2 one shows a higher fatigue limit, and also a much

larger number of cycles to failure for fatigue tests at the same stress amplitudes. According to Siddiqui et al. (2006), this mechanical behavior could be attributed to a softening mechanism of the 36CTR4 steel due to high-temperature tempering, along with a change in the microstructure from a martensite phase to a sorbitic one. Moreover, the 36CTR4 steel exhibits a much lower fatigue limit compared to the 27MnCrB5-2 one, but also a limited scatter of fatigue data as emphasized by the scatter bands in Figure 4.

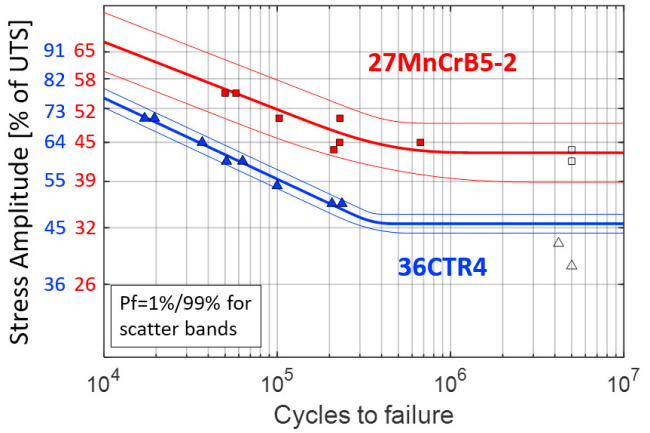

Fig. 4: S-N curves and scatter bands for the 27MnCrB5-2 and 36CTR4 steels. Values of stress amplitudes are intentionally masked to protect intellectual property; specifically, they are reported as % of UTS.

3.3. Fractographic Analyses

Figure 5 collects representative SEM micrographs at low magnification of the fracture surfaces of two selected fatigue specimens tested at the same stress amplitude of 700 MPa. In both steels, cracks initiated from single or multiple sites located at the surface, as pointed out by the white arrows in Figures 5a and b. The fatigue specimen of Figure 5a shows evidence of a ratchet mark due to presence of two adjacent crack origins that grew and linked together during the crack propagation phase. In addition to the propagation region, the final fatigue failure zone appears fibrous in both specimens.

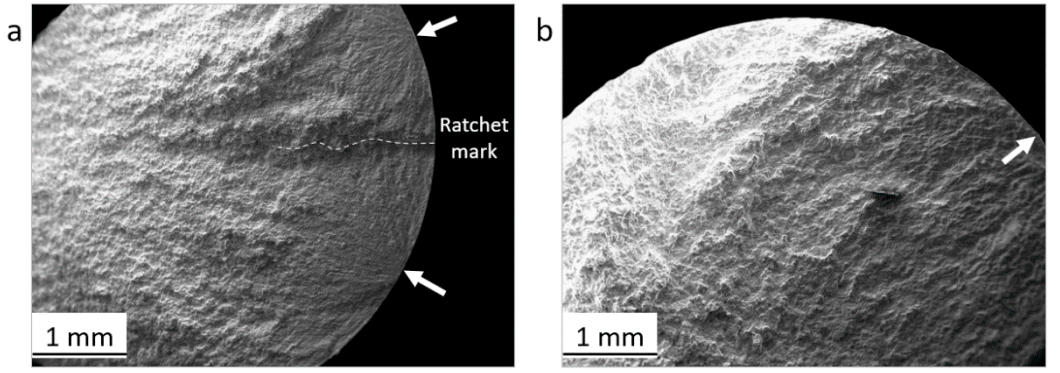

Fig. 5: SE-SEM micrographs (50× magnification) of fracture surfaces cut out from fatigue specimens made of (a) 27MnCrB5-2 and (b) 36CTR4 steels. White arrows indicate crack initiation points on the specimen external surface.

At higher magnification, fatigue striations were observed in both specimens, even though in the high-strength 27MnCrB5-2 steel (Figure 6a), which was tempered at low temperature, the striations were less distinct than those observed in the 36CTR4 steel (Figure 6b). Figures 7a and b collect SEM micrographs of the region corresponding to the final failure for the specimen made of the 27MnCrB5-2 steel, revealing dimples characteristics of a ductile failure

mechanism. Non-metallic inclusions were detected on the fracture surface and identified as manganese sulphides (MnS) and titanium nitrides (TiN), as confirmed by the EDS analyses (see EDS spectra of Figures 7c and d). The MnS particles are the most common inclusions in commercial steels and provide sites for the nucleation of microvoids and the subsequent formation of dimples (Murty et al. (1975); Joshi et al. (1975); Wang et al. (2016)). The presence of TiN inclusions suggested that the formation of B compounds was prevented, thus improving strength and hardenability of both Q&T steels, according to the findings of Turkdogan (1989) and Li et al. (2015). Moreover, similar amount of dimples and non-metallic inclusions were observed within the final failure region of the fracture surface for the 36CTR4 steel (see micrographs and EDS spectra of Figure 8).

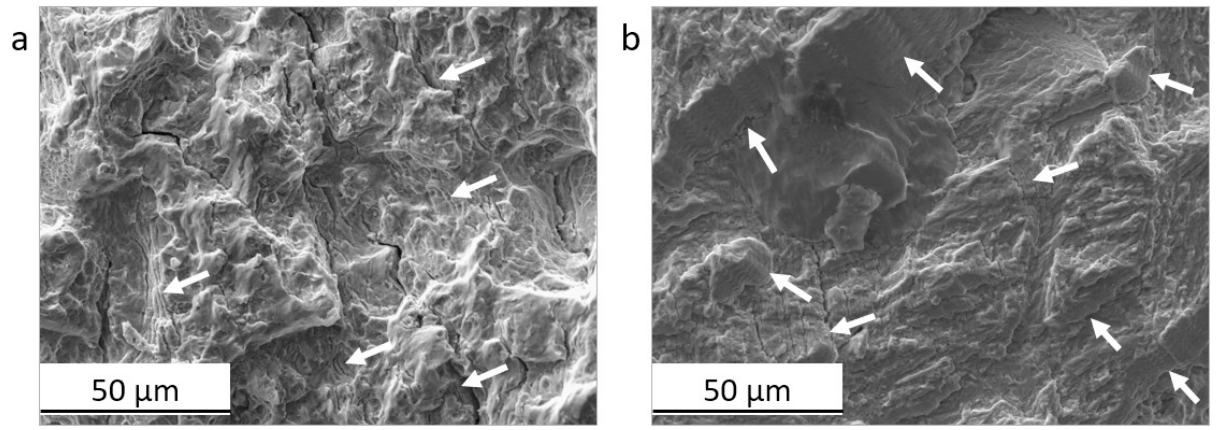

Fig. 6: SE-SEM micrographs (2000× magnification) showing details of fatigue striations (white arrows) within crack propagation zone of fatigue specimens made of (a) 27MnCrB5-2 and (b) 36CTR4 steels.

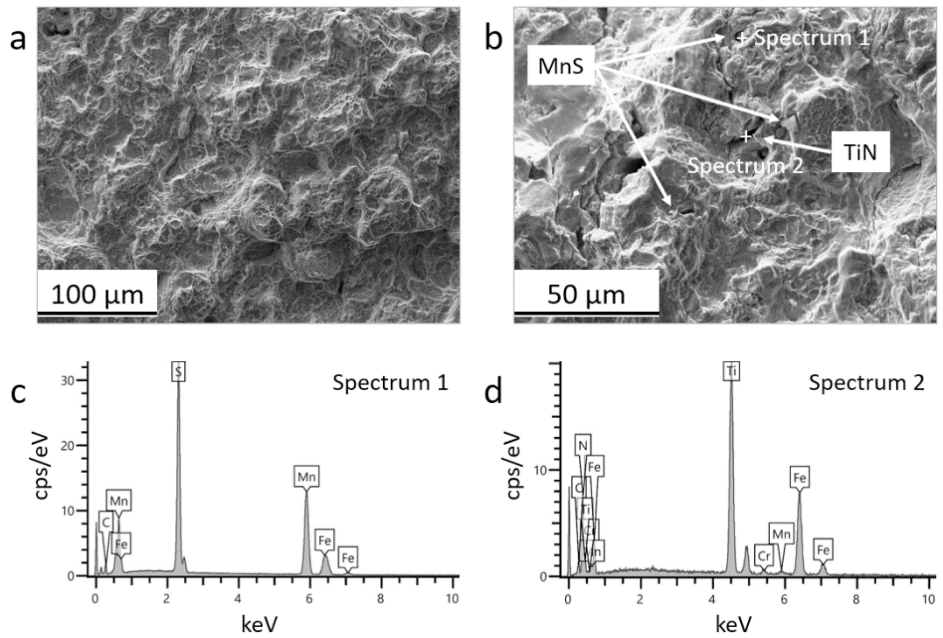

Fig. 7: (a, b) SE-SEM micrographs highlighting the presence of dimples within final failure region of the fatigue specimen made of 27MnCrB5-2 steel; (c, d) EDS spectra of some non-metallic inclusions detected within the same fracture surface.

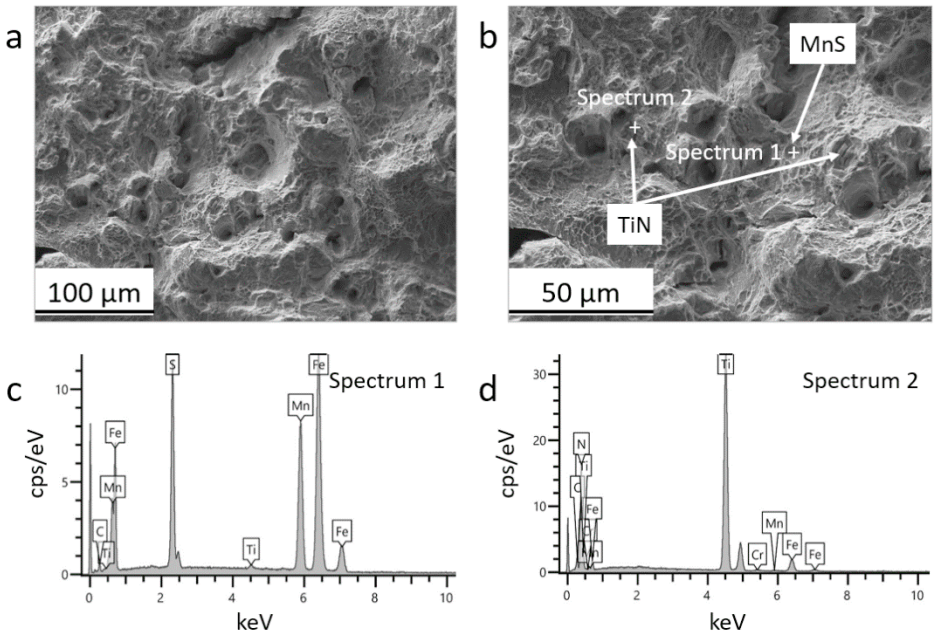

Fig. 8: (a, b) SE-SEM micrographs highlighting the presence of dimples within final failure region of the fatigue specimen made of 36CTR4 steel; (c, d) EDS spectra of some non-metallic inclusions detected within the same fracture surface.

4. Conclusions

In this study, a preliminary comparison of the fatigue behavior of 27MnCrB5-2 and 36CTR4 Q&T steels - both employed for the industrial production of undercarriage track links and subjected to a low- and high-temperature tempering, respectively - was carried out. The following general considerations can be drawn:

- The microstructural analyses proved that the 27MnCrB5-2 steel, tempered at low temperature according to a more sustainable heat treatment route, exhibited a matrix which agrees with a second stage tempered martensite. Conversely, the carbon neutral 36CTR4 steel showed a sorbitic microstructure, consistent with high-temperature tempering performed within the fourth stage.
- The microstructure resulting from low-temperature tempering of the 27MnCrB5-2 steel is characterized by higher strength and hardness compared with the 36CTR4 one, the latter exhibiting greater ductility due to tempering performed in the range 450÷550 °C. Hardness measurements carried out on both the transversal and longitudinal sections of broken tensile specimens confirmed the proper execution of both the forging process and the post-fabrication heat treatments.
- The 27MnCrB5-2 steel exhibited superior fatigue performance compared to the 36CTR4 one, as evidenced by its higher fatigue limit and larger number of cycles to failure at the same values of stress amplitude. In this case, the lower tempering temperature played a key role in improving fatigue strength of the 27MnCrB5-2 steel.
- Fractographic analyses confirmed that cracks initiated at single or multiple sites at the specimen surface for both the investigated Q&T steels. Fatigue striations were detected in the propagation zone within the facture surface of both steels, although they are more clearly visible in the 36CTR4 one. Non-metallic inclusions, such as Mn sulphides and Ti nitrides, were identified and associated with microvoid nucleation.

The preliminary results discussed in this work are useful for comparing the fatigue performance of two steels currently used in the industrial production of landing gear track links and subjected to traditional heat treatment parameters. A third steel is currently being tested, and its performance will be compared with the steels studied in this work. The research is still ongoing and new heat treatment routes are under investigation with the aim to reduce the environmental impact of the industrial heat treatments, without sacrificing the fatigue resistance.

Acknowledgements

The research activities in this study were conducted with the financial support of the CCIAA 2023 project of the University of Ferrara entitled “Acciai tradizionali e carbon neutral per componenti meccanici di machine operatrici industriali: dall’ottimizzazione del trattamento termico alla valutazione delle proprietà meccaniche per una economia più sostenibile” (Application ID 1755123).

References

ASTM E466, 2021. Standard practice for conducting force controlled constant amplitude axial fatigue tests of metallic materials. ASTM International, West Conshohocken, PA.

ASTM E8/E8M, 2021. Standard test methods for tension testing of metallic materials. ASTM International, West Conshohocken, PA.

Bastidas, D.M., Gil, A., Martin, U., Ress, J., Bosch, J., Medina, S.F., 2021. Failure analysis of boron steel 27MnCrB5 2 structural bolts during tightening of railcar wheel axle. Engineering Failure Analysis 124, 105333.

Cova, M., Tovo, R., 2017. Fitting fatigue data with a bi-conditional model. Fatigue & Fracture of Engineering Materials & Structures 40, 732–748.

Croccolo, D., De Agostinis, M., Ceschini, L., Morri, A., Marconi, A., 2013. Interference fit effect on improving fatigue life of a holed single plate. Fatigue & Fracture of Engineering Materials & Structures 36, 721–727.

Dudko, V., Yuzbekova, D., Gaidar, S., Vetrova, S., Kaibyshev, R., 2022. Tempering behavior of novel low-alloy high-strength steel. Metals 12, 1361.

ISO 6507-1, 2023. Metallic materials – Vickers hardness test – Part 1: Test method. International Organization for Standardization, Geneva.

ISO 683-2, 2012. Heat-treatable steels, alloy steels and free-cutting steels – Part 2: Technical delivery conditions for alloy steels for quenching and tempering. International Organization for Standardization, Geneva.

ISO 6892-1, 2019. Metallic materials – Tensile testing – Part 1: Method of test at room temperature. International Organization for Standardization, Geneva.

Joshi, A., Palmberg, P.W., Stein, D.F., 1975. Role of Mn and Si in temper embrittlement of low alloy steels. Metallurgical and Materials Transactions A 6, 2160–2161.

Larrañaga-Otegui, A., Pereda, B., Jorge-Badiola, D., Gutiérrez, I., 2016. Austenite static recrystallization kinetics in microalloyed B steels. Metallurgical and Materials Transactions A 47, 3150–3164.

Lee, W.S., Su, T.T., 1999. Mechanical properties and microstructural features of AISI 4340 high-strength alloy steel under quenched and tempered conditions. Journal of Materials Processing Technology 87, 198–206.

Li, C., Li, S., Duan, F., Wang, Y., Zhang, Y., He, D., Li, Z., Wang, W., 2017. Statistical analysis and fatigue life estimations for quenched and tempered steel at different tempering temperatures. Metals 7 (8), 312.

Li, Y., Ponge, D., Choi, P., Raabe, D., 2015. Segregation of boron at prior austenite grain boundaries in a quenched martensitic steel studied by atom probe tomography. Scripta Materialia 96, 13–16.

London, B., Nelson, D.V., Shyne, C., 1989. The influence of tempering temperature on small fatigue crack behavior monitored with surface acoustic waves in quenched and tempered 4140 steel. Metallurgical and Materials Transactions A 20, 1257–1265.

Mohrbacher, H., 2018. Property optimization in as-quenched martensitic steel by molybdenum and niobium alloying. Metals 8, 234.

Murty, Y.V., Morral, J.E., Kattamis, T.Z., Mehrabian, R., 1975. Initial coarsening of manganese inclusion. Metallurgical and Materials Transactions A 6, 2031–2039.

Shigesato, G., Fujishiro, T., Hara, T., 2014. Grain boundary segregation behavior of boron in low-alloy steel. Metallurgical and Materials Transactions A 45, 1876–1882.

Siddiqui, R.A., Qamar, S.Z., Pervez, T., Abdul-Wahab, S.A., 2006. Effect of heat treatment and surface finish on fatigue fracture characteristics in 0.45% carbon steel. Proceedings of the 10th International Research/Expert Conference Trends in the Development of Machinery and Associated Technology (TMT 2006), Barcelona-Lloret de Mar, Spain, pp. 153–156.

Speich, G.R., Leslie, W.C., 1972. Tempering of martensite. Metallurgical and Materials Transactions A 3, 1043–1054.

Turkdogan, E.T., 1989. Causes and effects of nitride and carbonitride precipitation during continuous casting. Iron & Steelmaker 16, 61–75.

Valtonen, K., Ojala, N., Haiko, O., Kuokkala, V., 2019. Comparison of various high-stress wear conditions and wear performance of martensitic steels. Wear 426–427, 3–13.

Wang, J., Liu, W., Yang, S., Liu, Q., Qi, Z., Li, J., 2016. Evolution and multidimensional characterization of non-metallic inclusions in steel: an industrial study. Metallurgical and Materials Transactions A 47, 6095–6107.